

Superconductivity in $\text{CuIr}_{2-x}\text{Al}_x\text{Te}_4$ telluride chalcogenides*

Dong Yan (严冬)^{1,4#}, Lingyong Zeng (曾令勇)^{1#}, Yijie Zeng (曾宜杰)^{2,5}, Yishi Lin (林一石)³, Junjie Yin (殷俊杰)², Meng Wang (王猛)², Yihua Wang (王熠华)³, Dao-Xin Yao (姚道新)² and Huixia Luo (罗惠霞)^{1†}

¹*School of Materials Science and Engineering, State Key Laboratory of Optoelectronic Materials and Technologies, Key Lab of Polymer Composite & Functional Materials, Guangzhou Key Laboratory of Flexible Electronic Materials and Wearable Devices, Sun Yat-Sen University, No.*

135, Xingang Xi Road, Guangzhou, 510275, P. R. China

²*Center for Neuron Science and Technology, School of Physics, Sun Yat-Sen University, No. 135,*

Xingang Xi Road, Guangzhou, 510275, P. R. China

³*State Key Laboratory of Surface Physics and Department of Physics, Fudan University, Shanghai 200433, P. R. China; Shanghai Research Center for Quantum Sciences, Shanghai 201315, China*

⁴*Key Laboratory of Functional Molecular Solids, Ministry of Education, College of Chemistry and Materials Science, Anhui Normal University, Wuhu, 241002, China*

⁵*College of Science, Hangzhou Dianzi University, Hangzhou 310018, P. R. China*

These authors contributed equally to this work.

The relationship between charge-density-wave (CDW) and superconductivity (SC), two vital physical phases in condensed matter physics, has always been the focus of scientists' research over the past decades. Motivated by this research hotspot, we systematically studied the physical properties of the layered telluride chalcogenide superconductors $\text{CuIr}_{2-x}\text{Al}_x\text{Te}_4$ ($0 \leq x \leq 0.2$). Through the resistance and magnetization measurements, we found that the CDW order was destroyed by a small amount of Al doping. Meanwhile, the superconducting transition temperature (T_c) kept changing with the change of doping amount and rose towards the maximum value of 2.75 K when $x = 0.075$. The value of normalized specific heat jump ($\Delta C/\gamma T_c$) for the highest T_c sample $\text{CuIr}_{1.925}\text{Al}_{0.075}\text{Te}_4$ was 1.53, which was larger than the BCS value of 1.43 and showed that bulk superconducting nature. In order to clearly show the relationship between SC and CDW states, we propose a phase diagram of T_c vs. doping content.

Keywords: Layered telluride chalcogenide; Superconductivity; Charge-density-wave; $\text{CuIr}_{2-x}\text{Al}_x\text{Te}_4$

PACS: 74.70.Xa; 74.25.-q; 74.25.Dw; 71.45.Lr

* H. X. Luo acknowledges the financial support by the National Natural Science Foundation of China (Grants No.11922415), Guangdong Basic and Applied Basic Research Foundation (2019A1515011718), and the Pearl River Scholarship Program of Guangdong Province Universities and Colleges (20191001). Y. Zeng and D. X. Yao are supported by the National Natural Science Foundation of China (Grants No. 11974432), NKRDPC-2018YFA0306001, NKRDPC-2017YFA0206203. D. Yan acknowledges the financial support by National Key Laboratory Development Fund (No. 20190030). Y. H. Wang would like to acknowledge partial support by the Ministry of Science and Technology of China under Grant No. 2017YFA0303000, NSFC Grant No. 11827805 and Shanghai Municipal Science and Technology Major Project Grant No. 2019SHZDZX01. M. Wang was supported by the National Natural Science Foundation of China (Grants No. 11904414, 12174454) and National Key Research and Development Program of China (Grants No. 2019YFA0705702).

† Corresponding author. E-mail: luohx7@mail.sysu.edu.cn

1. Introduction

The continuous suppression of metal-insulator (MI), charge-density-wave (CDW) transition and magnetism, etc. leading to the occurrence of superconductivity (SC) in the proximity of such quantum states has garnered great interest and widespread study in solid-state physics.^[1-4] The phase diagrams of unconventional high-temperature (high- T_c) cuprates and iron-based superconductors exemplified such phenomena.^[5-11] Nevertheless, how SC emerges in these high- T_c superconductors are intricate and remains extremely puzzling. It is still essential to sort out the interplay between the SC and the other quantum states, promoting further understanding of the mechanism of high- T_c superconductors.

Low-dimensional layered transition metal dichalcogenides (TMDs) are other opportune material platforms for the exploration of various quantum instabilities,^[12-21] especially the interplay between SC and CDW, in which the CDW order refers to condensate with periodic modulations of the crystalline lattice and conduction electron density in real space. Typically, the SC can be induced and a dome-shape superconducting phase diagram is formed upon suppressing the CDW order,^[22-27] which is highly similar to the phase diagrams of unconventional high- T_c cuprates and iron-based superconductors. Despite overall phase diagram similarities, there are significant differences especially between their mechanisms, where unconventional high- T_c Fe-based and cuprate superconductors cannot be well explained by Bardeen-Cooper-Schrieffer (BCS) theory but most of the TMD superconductors can be explained by BCS theory. It has been generally considered that the collapse of CDW state accompanied by the improvement of superconducting transition temperature (T_c) is in reference to the abrupt enhancement of density of states (DOS) around the Fermi level $N(E_F)$ in the conventional superconductors owing to CDW state gaps out some regions of the Fermi surface.^[1,2] The formation of Cu_xTiSe_2 ($0 \leq x \leq 0.1$) from intercalating the Cu into 1T-TiSe₂ exemplified a vivid phase diagram in the TMDs family,^[2] and further evoked the continuous interest in searching for new superconductors in TMD materials by gating, adding physical pressures, chemical doping or point contact method.^[22-38] For example, Cu-intercalation 2H-TaS₂ forms Cu_xTaS_2 ($0 \leq x \leq 0.12$) and displays an enhancement of T_c from 0.8 K ($x = 0$) to 4.5 K ($x = 0.04$).^[34] In addition, experiments show that the T_c of WTe₂ can be increased to 7 K under an applied physical pressure of 16.8 GPa.^[35] Moreover, manifold phase transitions from MI to metal show in 1T-TaS₂ thin flakes with collapses of CDWs, and finally SC is induced by ionic gating.^[36]

Currently, CuIr_2Te_4 , adopting a NiAs defected structure of trigonal symmetry with the space group $P-3m1$, has been found to exhibit the coexistence of the CDW-like transition ($T_{\text{CDW}} = 250$ K on heating and 186 K on cooling) and SC ($T_c = 2.5$ K). Besides, recent electronic structure calculations have unveiled that the Fermi energy is mostly derived from Ir $5d$ and Te $5p$ orbitals.^[39] More recently, experiments have documented that both CDW and SC performances of CuIr_2Te_4 can be modified via $3d$, $4d$ transition metals (e.g., Ti and Ru) and $4p$, $5p$ dopants (e.g., Se and I). Dome-shape phase diagrams with respect to T_c vs. doping amount associated with the suppression of CDW have been found in the $\text{CuIr}_{2-x}\text{Ru}_x\text{Te}_4$ and $\text{CuIr}_{2-x}\text{Ti}_x\text{Te}_4$ systems, but dome-shape diagrams

crowded in the middle doping region with two CDW regions at two sides in Se and I-doped systems. [40-43] Furthermore, the non-magnetic element Al is usually selected as the dopant because Al^{3+} ion has a closed shell electron configuration and a clear oxidation state. The transport properties of Al-doped high- T_c copper-based superconductors (e.g. $\text{SmBa}_2\text{Cu}_{3-x}\text{Al}_x\text{O}_{6+\delta}$, $\text{YBa}_2\text{Cu}_{3-x}\text{Al}_x\text{O}_7$) has been widely studied. [44, 45] And nano Al has been used to improve the critical current in MgB_2 superconductor. [46] Therefore, it will be interesting to explore the effect of 3s dopants (e.g., Al) on the CDW and SC in CuIr_2Te_4 .

In this work, we prepared the polycrystalline $\text{CuIr}_{2-x}\text{Al}_x\text{Te}_4$ ($0 \leq x \leq 0.2$) compounds successfully by a solid-state reaction method. Our results demonstrate that the CDW order can be completely suppressed within a fine-tuned Al-doped content as a result of the improvement of T_c . T_c initially increases with the rise of doping amount until $x = 0.075$ and reaches highest value of 2.75 K, eventually forming a dome-phase like electronic phase diagram. The acquisition of the $\text{CuIr}_{2-x}\text{Al}_x\text{Te}_4$ ($0 \leq x \leq 0.2$) system also provides some enlightenment for the search of new superconductors.

2. Experimental Methods

Synthesis: Polycrystalline specimens of $\text{CuIr}_{2-x}\text{Al}_x\text{Te}_4$ ($0 \leq x \leq 0.2$) were prepared through the classical solid-state phase reaction. First, the Cu (99%, Alfa Aesar), Ir (99.9%, Macklin), and Al (99.95%, Aladdin) powder, and Te lump (99.999%, Alfa Aesar) with an element ratio of Cu : Ir : Al : Te = 1 : 2-x : x : 4.05 was sealed in quartz tubes, then put them in a muffle furnace with the ramping rate 1 °C/min to 850 °C and maintain the temperature for 5 days. The resulting samples were annealed at 850 °C for 4 days with a heating rate 1 °C/min.

Instruments: Powder X-ray diffraction (PXRD) MiniFlex, Rigaku with $\text{Cu } K\alpha 1$ radiation was used to examine the crystal structure and phase purity for $\text{CuIr}_{2-x}\text{Al}_x\text{Te}_4$ ($0 \leq x \leq 0.2$) compounds. FULLPROF software suite was used to determine the cell parameters based on Thompson-Cox-Hastings pseudo-Voigt peak shapes model. Measurements of the temperature-dependence of electrical resistivity, specific heat, and magnetic susceptibilities ($M(T, H)$) were performed by a DynaCool Quantum Design Physical Property Measurement System (PPMS, Quantum Design, Inc.)

3. Results and Discussion

The PXRD patterns of $\text{CuIr}_{2-x}\text{Al}_x\text{Te}_4$ compounds are presented in **Fig. 1a**. PXRD analysis shows that Al concentration is limited up to 0.2 since Al_2Te_3 impurity is found with further increasing Al content. As Al doping content increases, the (001) peak moves to the right, which can be verified by the decrease of lattice constants a and c with increasing x (**Fig. 1c**), reflecting the compression of the CuIr_2Te_4 unit cell. As illustrated in **Fig. 1c**, clearly, both lattice constants (a and c) and c/a singly reduce with increasing Al concentration. It is found that a and c reduce from 3.9397(5) and 5.3965(3) Å for the pristine sample to 3.9264(1) and 5.3757(2) Å ($x = 0.2$) in $\text{CuIr}_{2-x}\text{Al}_x\text{Te}_4$, respectively. The detailed refinement of the selected sample $\text{CuIr}_{1.925}\text{Al}_{0.075}\text{Te}_4$ is displayed in **Fig. 2a**. Most of the diffraction peaks have been indexed in terms of trigonal symmetry with a space group $P-3m1$ (No. 164) and some small peaks indexed

for tiny unreacted Ir are also detected. The illustration shows that the disordered trigonal structure, in which the Cu is inserted between two-dimensional (2D) IrTe₂ layers, Ir partial substituting by Al simultaneously (see Fig. 2b and 2c).

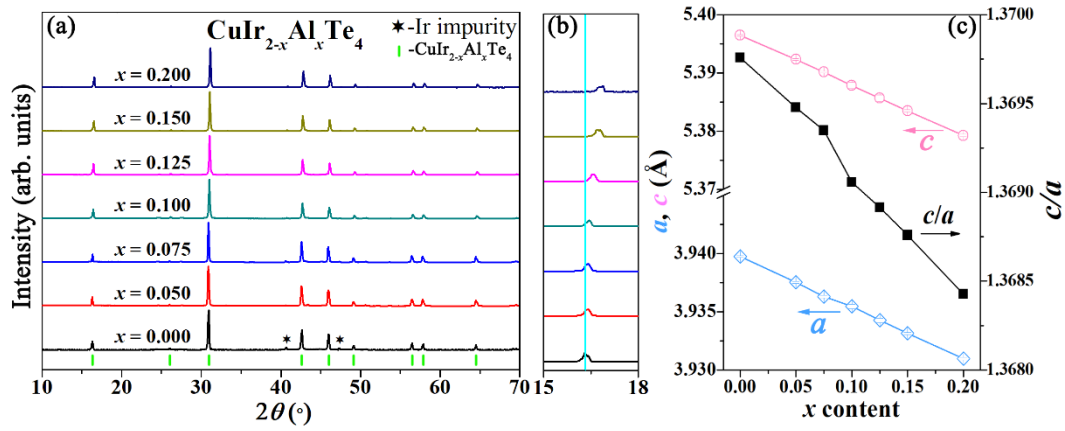


Fig. 1 (a) and (b) displays PXRD patterns of the $\text{CuIr}_{2-x}\text{Al}_x\text{Te}_4$ ($0 \leq x \leq 0.2$) compounds. (c) The evolution of lattice constants for $\text{CuIr}_{2-x}\text{Al}_x\text{Te}_4$ ($0 \leq x \leq 0.2$).

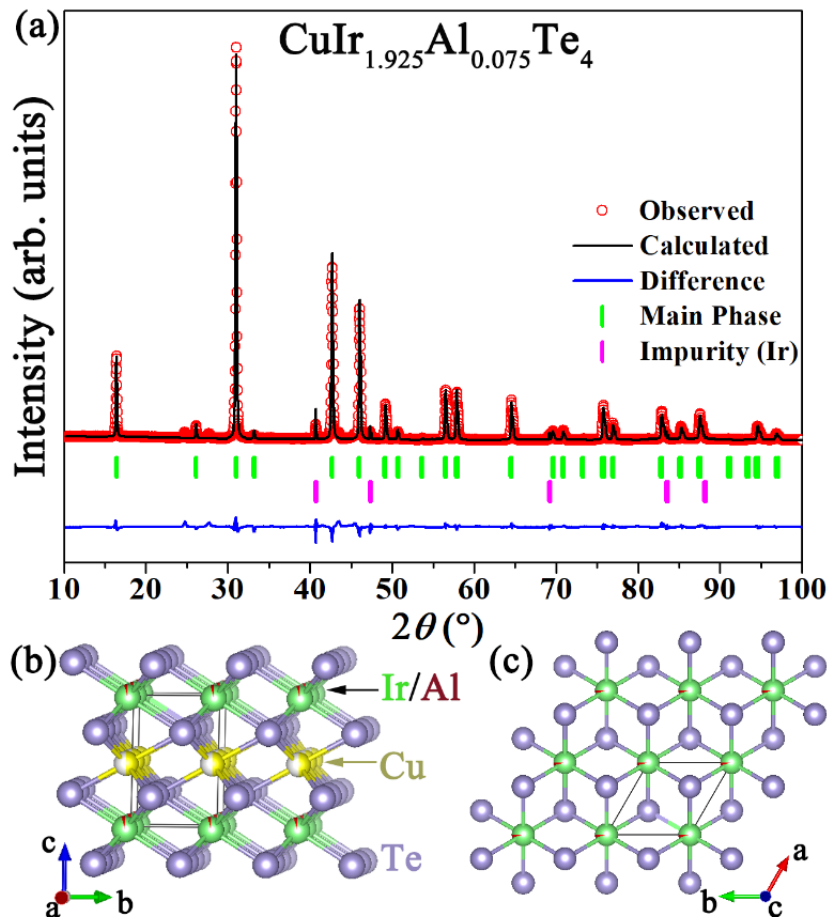


Fig. 2 (a) Refinements of $\text{CuIr}_{1.925}\text{Al}_{0.075}\text{Te}_4$ polycrystalline sample. (b) and (c) show the crystal structure of $\text{CuIr}_{2-x}\text{Al}_x\text{Te}_4$ in different direction views.

Table 1. T_c and RRR of $\text{CuIr}_{2-x}\text{Al}_x\text{Te}_4$ ($0 \leq x \leq 0.2$) compounds. The T_c is determined by using

50% normal state resistance criterion.

| x content | T_c (K) | RRR |
|-------------|-----------|-------|
| 0 | 2.50 | 4.149 |
| 0.05 | 2.74 | 4.367 |
| 0.075 | 2.75 | 4.444 |
| 0.1 | 2.72 | 4.115 |
| 0.125 | 2.71 | 2.865 |
| 0.15 | 2.41 | 3.846 |
| 0.2 | | 2.342 |

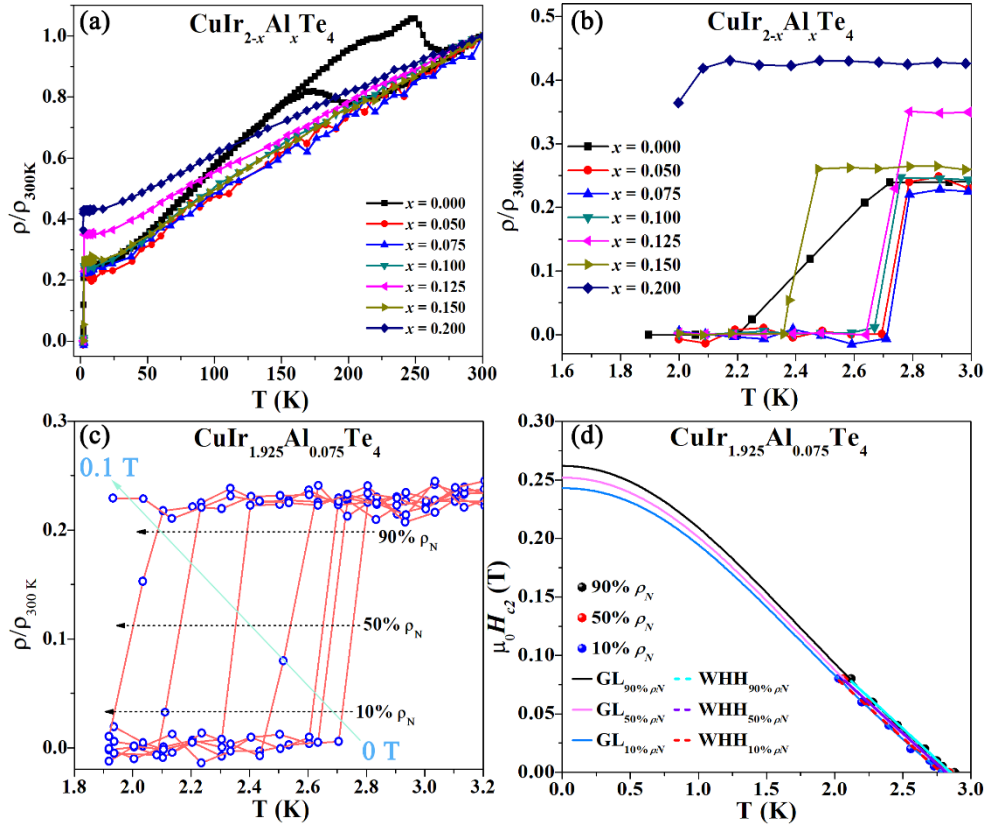


Fig. 3 (a) Temperature-dependence of resistivity for the polycrystalline $\text{CuIr}_{2-x}\text{Al}_x\text{Te}_4$ ($0 \leq x \leq 0.2$) compounds. (b) The superconducting transition at 1.6 - 3.0 K for the polycrystalline $\text{CuIr}_{2-x}\text{Al}_x\text{Te}_4$ ($0 \leq x \leq 0.2$) compounds. (c) Temperature dependences of resistivity for the polycrystalline $\text{CuIr}_{1.925}\text{Al}_{0.075}\text{Te}_4$ sample under various applied magnetic fields. (d) Temperature dependence of H_{c2} for the polycrystalline $\text{CuIr}_{1.925}\text{Al}_{0.075}\text{Te}_4$ sample.

The temperature-dependent normalized resistivity (ρ/ρ_{300K}) of the $\text{CuIr}_{2-x}\text{Al}_x\text{Te}_4$ ($0 \leq x \leq 0.2$) compounds is exhibited in **Fig. 3a**. Besides, our previous finding indicates that there is no structure transition for the pristine sample. Thus, we propose that the normalized resistivity with cooling and heating exhibited a distinct hysteresis associated with the formation of CDW-like transition for the pristine CuIr_2Te_4 sample. It is worth mentioning that no signature of the abnormal hump can be observed above T_c in ρ/ρ_{300K} of the Al doping samples $\text{CuIr}_{2-x}\text{Al}_x\text{Te}_4$ ($0 < x \leq 0.2$), indicating the CDW-like transition can be suppressed with subtle Al substitution for Ir, accompanying with the increment of T_c . The resistivity data for Al-doped samples show a metallic behavior.

We can observe sharp drops of $\rho(T)$ for the $\text{CuIr}_{2-x}\text{Al}_x\text{Te}_4$ ($0 \leq x \leq 0.15$) below 3.0 K (see **Fig. 3b**), which represent the outset of the superconducting state. The transition width of Al-doped compounds is much narrower than that of the pristine CuIr_2Te_4 . The T_c and residual resistivity ratio (RRR = $R(300\text{K})/R(3\text{K})$) of $\text{CuIr}_{2-x}\text{Al}_x\text{Te}_4$ ($0 \leq x \leq 0.2$) samples summarized in **Table 1**. As Al content increases, both T_c and RRR increase to the highest value at $x = 0.075$, then decrease for further Al doping. For $0.075 \leq x \leq 0.5$, the RRR value sharply decreases from 4.44 for $x = 0.075$ to 2.342 for $x = 0.234$. This phenomenon indicates that high Al content induces significant disorder in the polycrystalline $\text{CuIr}_{2-x}\text{Al}_x\text{Te}_4$ series.

Table 2. Comparison of physical properties of CuIr_2Te_4 -based superconductors.

| Compound | $\text{CuIr}_{1.925}\text{Al}_{0.075}\text{Te}_4$ | $\text{CuIr}_{1.925}\text{Ti}_{0.075}\text{Te}_4$ [33] | $\text{CuIr}_{1.95}\text{Ru}_{0.05}\text{Te}_4$ [32] | CuIr_2Te_4 [31] |
|---|---|---|---|------------------------------------|
| T_c (K) | 2.75 | 2.84 | 2.79 | 2.50 |
| γ ($\text{mJ mol}^{-1} \text{K}^{-2}$) | 12.12 | 14.13 | 12.26 | 12.05 |
| β ($\text{mJ mol}^{-1} \text{K}^{-4}$) | 2.20 | 2.72 | 1.87 | 1.97 |
| Θ_D (K) | 183.5(1) | 170.9(1) | 193.6(2) | 190.3(1) |
| $\Delta C/\gamma T_c$ | 1.53 | 1.34 | 1.51 | 1.50 |
| λ_{ep} | 0.66 | 0.64 | 0.65 | 0.63 |
| $N(E_F)$ (states/eV f.u.) | 3.13 | 3.67 | 3.15 | 3.10 |
| $\mu_0 H_{c2}(T)$ (50 % ρ_N WHH theory) | 0.191 | 0.212 | 0.247 | 0.12 |
| $\mu_0 H^P(T)$ | 5.12 | 5.28 | 5.24 | 4.65 |
| $\mu_0 H_{c1}(T)$ | 0.060 | 0.095 | 0.098 | 0.028 |
| $\xi_{GL}(0)$ (nm) (50 % ρ_N WHH theory) | 40.4 | 39.3 | 36.3 | 52.8 |

To evaluate the superconducting properties of $\text{CuIr}_{1.925}\text{Al}_{0.075}\text{Te}_4$ compound with the highest T_c in detail, we have measured the resistivity under various applied magnetic fields. T_c s shift to lower temperature with the increasing applied field (see in **Fig. 3c**). The upper critical field $\mu_0 H_{c2}(0)$ is obtained from Werthamer-Helfand-Hohenberg (WHH) and Ginzburg-Landau (GL) models. The upper critical field $\mu_0 H_{c2}(T)$ values of $\text{CuIr}_{1.925}\text{Al}_{0.075}\text{Te}_4$ at zero temperature can be extrapolated by GL formula using the data deriving from 10, 50, and 90 % criteria of ρ_N (normal-state resistivity). The GL formula is shown as follows: $\mu_0 H_{c2} = \mu_0 H_{c2}(0) * \frac{1-(T/T_c)^2}{1+(T/T_c)^2}$.^[47] The $\mu_0 H_{c2}(0)$ values of 0.235, 0.250, and 0.255 T for $\text{CuIr}_{1.925}\text{Al}_{0.075}\text{Te}_4$ can be determined using the data 10, 50 and 90 % criteria of ρ_N , respectively. Furthermore, we can acquire $\mu_0 H_{c2}(0)$ values of 0.180, 0.191, and 0.193 T for $\text{CuIr}_{1.925}\text{Al}_{0.075}\text{Te}_4$ corresponded to the data 10, 50, and 90 % criteria of ρ_N , respectively, via using the WHH formula $\mu_0 H_{c2} = -0.693 T_c \frac{dH_{c2}}{dT_c}$ for the dirty limit SC.^[48] The slopes, dH_{c2}/dT , are obtained from linear fitted $\text{CuIr}_{1.925}\text{Al}_{0.075}\text{Te}_4$ sample for data 10, 50 and 90 % criteria of ρ_N . Additionally, we fit the Pauli limiting field ($\mu_0 H^P(T)$) by the formula $\mu_0 H^P(T) = 1.86 T_c$, which is shown in **Table 2**. Then, the Ginzburg-Landau coherence length $\xi_{GL}(0)$ can be derived from this

equation $\mu_0 H_{c2}(T) = \frac{\phi_0}{2\pi\xi_{GL}^2}$, where ϕ_0 represents the flux quantum. For example, $\xi_{GL}(0)$ of $\text{CuIr}_{1.925}\text{Al}_{0.075}\text{Te}_4$ is calculated to be 40.4 nm via using 50 % criteria of ρ_N data based on WHH model. **Table 2** summarizes all the relative experimentally measured and estimated parameters.

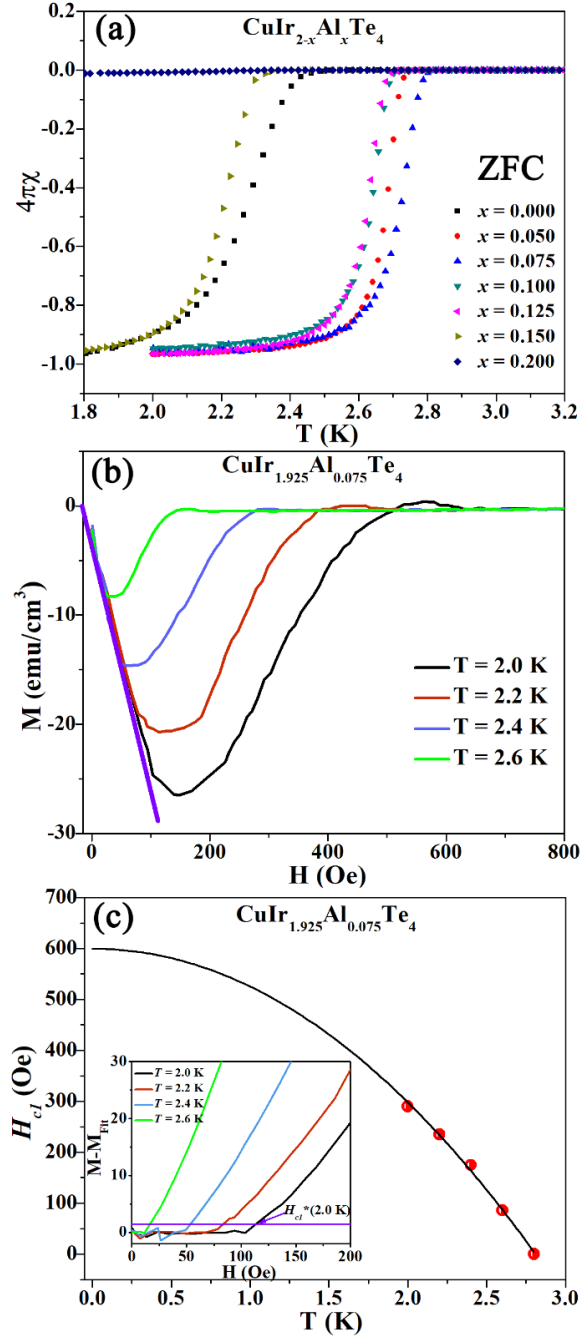


Fig. 4 (a) Magnetic susceptibility for $\text{CuIr}_{2-x}\text{Al}_x\text{Te}_4$ ($0 \leq x \leq 0.2$) compounds under 30 Oe magnetic field with zero-field-cooling (ZFC) mode. (b) The magnetization $M(H)$ in a temperature range between 2 - 2.6 K of $\text{CuIr}_{1.925}\text{Al}_{0.075}\text{Te}_4$. (c) Temperature dependence of H_{c1} . Inset: Difference between M and M_{Fit} in a temperature range between 2 - 2.6 K of $\text{CuIr}_{1.925}\text{Al}_{0.075}\text{Te}_4$.

The superconducting transition has also been confirmed by the magnetic susceptibility data (**Fig. 4a**) with strong diamagnetic signals under zero-field-cooling (ZFC) mode. The superconducting volume fraction of the $\text{CuIr}_{2-x}\text{Al}_x\text{Te}_4$ ($0 \leq x \leq 0.15$) compounds can be calculated around 95 %, which manifests high purity of the polycrystalline $\text{CuIr}_{2-x}\text{Al}_x\text{Te}_4$ samples. Next, we examine the lower critical fields ($\mu_0 H_{c1}$) by the field-dependent magnetic susceptibility $M(H)$ measurements in a temperature range between 2 - 2.6 K. **Fig. 4b** presents the magnetization (M - H) curves at different temperatures below T_c of the representative $\text{CuIr}_{1.925}\text{Al}_{0.075}\text{Te}_4$. As shown in the purple line in **Fig. 4b**, the $M(H)$ isotherms show a linear relationship with the magnetic field (H) at low magnetic fields, indicating it is a type-II superconductor. We can extract the demagnetization factor (N) values following the expression: $N = 4\pi\chi_V + 1$, where $\chi_V = \frac{dM}{dH}$ represents the linearly fitted slope. The calculated N value for $\text{CuIr}_{1.925}\text{Al}_{0.075}\text{Te}_4$ is about 0.53. We can use the expression $M_{\text{fit}} = m + nH$ to fit the experimental data at low magnetic fields, where m represents the intercept and n stands for the slope of linear fitting from the low magnetic field $M(H)$ data. The inset of **Fig. 4c** displays the $(M - M_{\text{fit}})$ data vs. H . Then, we can fit the $\mu_0 H_{c1}(T)$ by the expression $\mu_0 H_{c1}(T) = \frac{\mu_0 H_{c1}^*(T)}{1 - N}$, where $\mu_0 H_{c1}^*$ is the intersection point between the $M - M_{\text{fit}}$ vs. H curves and the field (purple line in the inset of **Fig. 4c**), which deviates by $\sim 1\%$ above the fitted data (M_{fit}) as customary. The temperature dependence of $\mu_0 H_{c1}(T)$ for $\text{CuIr}_{1.925}\text{Al}_{0.075}\text{Te}_4$ is displayed in the main panel of **Fig. 4c**. Consequently, we can further acquire the $\mu_0 H_{c1}(T)$ using the equation $\mu_0 H_{c1}(T) = \mu_0 H_{c1}(0)(1 - (T/T_c)^2)$. The estimated $\mu_0 H_{c1}(0)$ at zero temperature of $\text{CuIr}_{1.925}\text{Al}_{0.075}\text{Te}_4$ sample is 0.060 T, which is larger than that of undoped parent sample (see in **Table 2**).

To further convince that SC is essential feature of the highest T_c compound $\text{CuIr}_{1.925}\text{Al}_{0.075}\text{Te}_4$, we also perform the temperature-dependent specific heat measurement. **Fig. 5** illustrates the detailed characterization of the superconducting transition in the highest T_c composition $\text{CuIr}_{1.925}\text{Al}_{0.075}\text{Te}_4$ through specific heat measurements under absence of magnetic field. The data C_p/T vs. T^2 can be fitted by the equation $C_p = \gamma T + \beta T^3$ above the T_c to acquire the value of β and γ is $2.20 \text{ mJ mol}^{-1} \text{ K}^{-4}$ and $12.12 \text{ mJ mol}^{-1} \text{ K}^{-2}$ for $\text{CuIr}_{1.925}\text{Al}_{0.075}\text{Te}_4$, respectively, where γT represents the sum of electron contributions (C_{el}) to the specific heat and βT^3 is the sum of phonon contributions (C_{ph}). **Fig. 5b** shows the sum of electron contribution to the specific heat at the temperature near the T_c under 0 T, where C_{el} is easily derived from deducting the phonon part: $C_{el} = C_p - \beta T^3$. Apparently, a sharp specific heat jump occurs in our representative $\text{CuIr}_{1.925}\text{Al}_{0.075}\text{Te}_4$, characteristic of bulk SC. The T_c further can be determined to be 2.70 K using the common equal-area entropy construction method, which agrees well with those observed in magnetization and resistivity tests. Based on the T_c and γ values, we can determine $\frac{\Delta C_{el}}{\gamma T_c} = 1.53$, which is slightly larger than the value of 1.43 forecasted by the BCS theory, revealing its superconducting nature. The

Debye temperature obtained using the equation $\Theta_D = (12\pi^4 nR/5\beta)^{1/3}$ is 183.5(1) K, where R represents the gas constant, n expresses the number of atoms per formula unit. The resultant electron-phonon coupling constant λ_{ep} value further estimated by introducing the Θ_D number into the inverted McMillan

equation: $\lambda_{ep} = \frac{1.04 + \mu^* \ln\left(\frac{\Theta_D}{1.45T_c}\right)}{(1 - 0.62\mu^*) \ln\left(\frac{\Theta_D}{1.45T_c}\right) - 1.04}$ [49] for $\text{CuIr}_{1.925}\text{Al}_{0.075}\text{Te}_4$ is 0.66. Following the

formula $N(E_F) = \frac{3}{\pi^2 k_B^2 (1 + \lambda_{ep})} \gamma$, the λ_{ep} and γ values can give rise to the electron density of states (DOSs) around the Fermi level ($N(E_F)$). The obtained $N(E_F) = 3.13$ states/eV f.u. for $\text{CuIr}_{1.925}\text{Al}_{0.075}\text{Te}_4$, greater than that of pristine CuIr_2Te_4 ($N(E_F) = 3.10$ states/eV f.u.). The enhancement of T_c may be accompanied by the increment of the DOS states at the Fermi energy in $\text{CuIr}_{2-x}\text{Al}_x\text{Te}_4$ systems. As show in **Fig. 5b**, the specific heat data can be basically fit with the equation $C_{el} = A \exp(-\Delta/(k_B T))$. Due to the limitation of experimental conditions, the specific heat measurement did not measure the lower temperature region. Nevertheless, the R^2 value of 0.9998 shows that the data and the calculated curve are reasonably consistent.

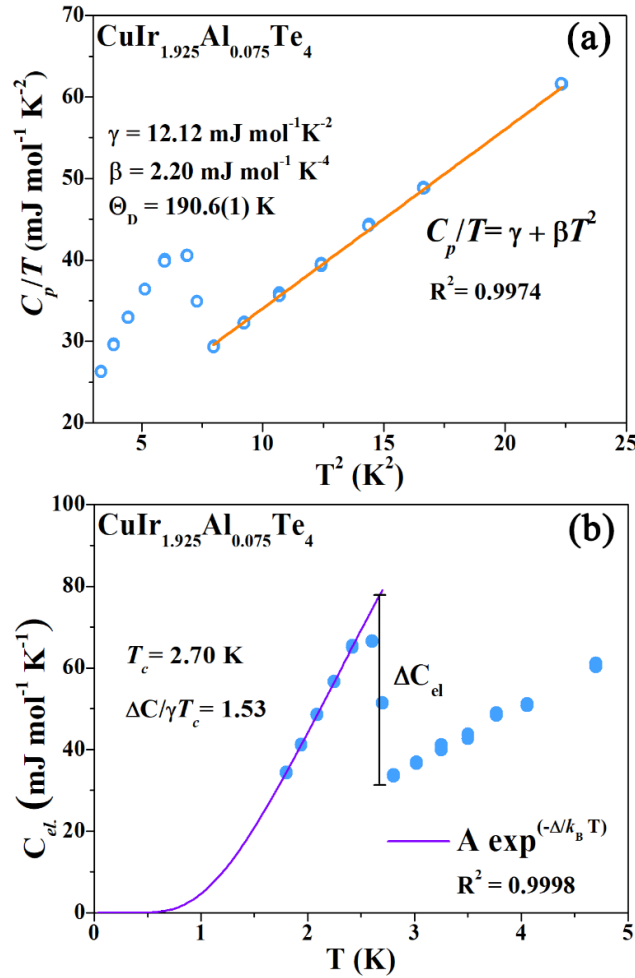


Fig. 5 (a) Specific heat data plotted as a function of T^2 for $\text{CuIr}_{1.925}\text{Al}_{0.075}\text{Te}_4$. (b) the electronic part of the specific heat in $\text{CuIr}_{1.925}\text{Al}_{0.075}\text{Te}_4$.

Finally, to further understand the effect of Al dopant on the CDW and SC of CuIr_2Te_4 , the electronic phase diagrams plotted T_c versus Al-content x have been established (see **Fig. 6**). All the T_c values were obtained from the resistivity and magnetization tests. From **Fig. 6**, we can find that the CDW order is immediately suppressed while T_c increases with increasing Al content up to $x = 0.075$ and rises towards the highest value 2.75 K at $x = 0.075$. From this, we find that despite subtle Al is instead of Ir, it has a strong impact on the SC and CDW. Besides, in contrast to our previously reported system Ru/Ti-doped CuIr_2Te_4 , the similarity is the destabilization of CDW upon small amount doping concentration no matter Ru, Ti, or Al as dopants and formation of dome-shape like superconducting phase diagrams. ^[32,33] Despite overall similarities, there are significant differences between the $\text{CuIr}_{2-x}\text{Ru}_x\text{Te}_4$, $\text{CuIr}_{2-x}\text{Ti}_x\text{Te}_4$, and $\text{CuIr}_{2-x}\text{Al}_x\text{Te}_4$ systems. Substitution of Ir by Ru or Ti in CuIr_2Te_4 corresponds to a “hole” (p -type) doping of the IrTe_2 layers, while partial doping Al into Ir site in CuIr_2Te_4 is an electron (n -type) doping. As for the high- T_c cuprate superconductors, where the competition between anti-ferromagnetism and SC develops as a function of chemical doping, the evolving balance between competing electronic orders in CDW/SC systems is one of their most fundamentally tempting properties. In our case, the bands in the neighborhood of the Fermi energy E_F of the pristine sample CuIr_2Te_4 mostly come from Ir d and Te p orbitals and locate at a flat plateau, in which Al doping acts as a chemical pressure, closing the gap on the Fermi surface that usually leads to rapid suppression of CDW. On the other hand, the increase of band filling of the Fermi surface under chemical pressure could be the mechanism of the promotion of SC. But further study and evidence need to be collected to find out the competition between CDW and SC.

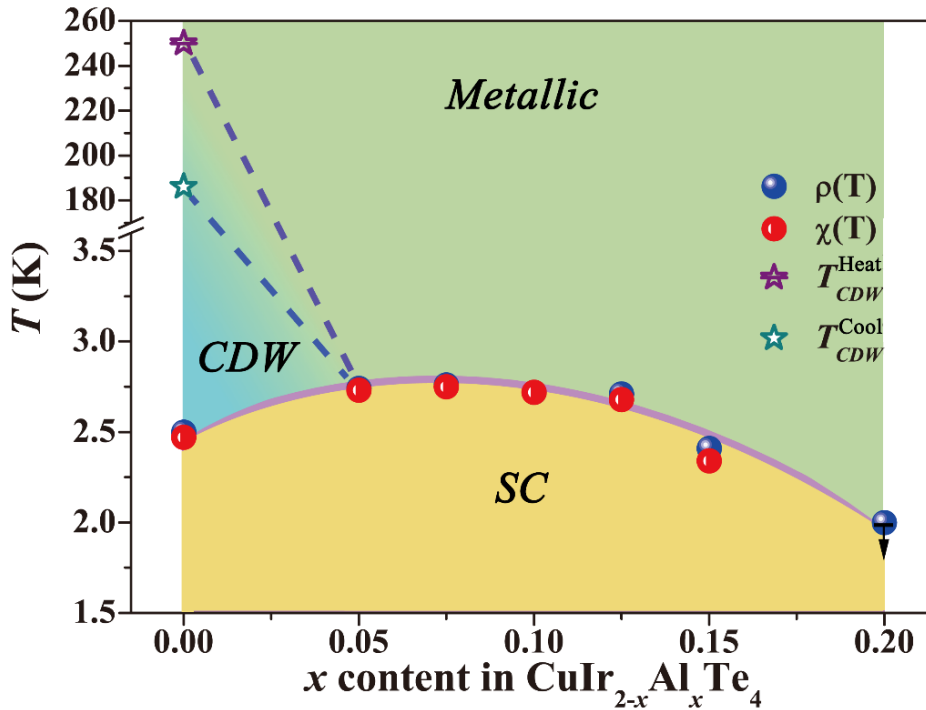


Fig. 6 The electronic phase diagram of polycrystalline $\text{CuIr}_{2-x}\text{Al}_x\text{Te}_4$ ($0 \leq x \leq 0.2$) series.

4. Conclusion and perspectives

In conclusion, we have successfully synthesized a series of polycrystalline $\text{CuIr}_{2-x}\text{Al}_x\text{Te}_4$ ($0 \leq x \leq 0.2$) samples via a solid-state method and systemically studied the effect of Al doping on the structure and electronic properties of CuIr_2Te_4 . The $\frac{\Delta C_{el}}{\gamma T_c} = 1.53$ for the highest T_c sample $\text{CuIr}_{1.925}\text{Al}_{0.075}\text{Te}_4$ is slightly larger than 1.43 (BCS value), proving its bulk superconducting nature. We recognize that the CDW order is suppressed immediately while T_c increases as Al doping amount x rises and achieves a maximum $T_c = 2.75$ K with Al doping content of 0.075. Our systematic study of $\text{CuIr}_{2-x}\text{Al}_x\text{Te}_4$ ($0 \leq x \leq 0.2$) not only extends the family of the TMD superconductors but also provides a platform for further research on the relationship between the CDW and SC.

References

1. Doan P, Gooch M, Tang Z J, Lorenz B, Möller A, Tapp J, Chu P C W and Guloy A M 2012 *J. Am. Chem. Soc.* 134 16520
2. Mososan E, Zandbergen H W, Dennis B S, Bos J W G, Onose Y, Klilmczuk T, Ramirez A P, Ong N P and Cava R J 2006 *Nat. Phys.* 2 544
3. Shen B, Du F, Li R, Thamizhavel A, Smidman M, Nie Z Y, Luo S S, Le T, Hossain Z and Yuan H Q 2020 *Phys. Rev. B* 101 144501
4. Fang L, Wang Y, Zou P Y, Tang L, Xu Z, Chen H, Dong C, Shan L and Wen H H 2005 *Phys. Rev. B* 72 014534
5. Zhao Z X, Chen L Q, Yang Q S, Huang Y Z, Chen G H, Tang R M, Liu G R, Cui C G, Chen L, Wang L Z, Guo S Q, Li S L and Bi J Q 1987 *Chin. Sci. Bull.* 32 412
6. Wu M K, Ashburn J R, Torng C J, Hor P H, Meng R L, Guo L, Huang Z J, Wang Y Q and Chu C W 1987 *Phys. Rev. Lett.* 58 908
7. Sasmal K, Lv B, Lorenz B, Guloy A M, Guloy F, Xue Y Y and Chu C W 2008 *Phys. Rev. Lett.* 101 107007
8. Chuang T M, Allan M P, Lee J, Xie Y, Ni N, Bud'ko, S L, Boebinger G S, Canfield P C and Davis J C 2010 *Science* 327 181
9. Ren Z A, Lu W, Yang J, Yi W, Shen X L, Li Z C, Che G C, Dong X L, Sun L L and Zhao Z X 2008 *Chin. Phys. Lett.* 25 2215
10. Mao Y Y, Li J, Huang Y L, Yuan J, Li Z A, Chai K, Ma M W, Ni S L, Tian J P, Liu S B, Zhou H X, Zhou F, Li J Q, Zhang G M, Jin K, Dong X L and Zhao Z X 2018 *Chin. Phys. Lett.* 35 057402
11. Yang J, Zhou R, Wei L L, Yang H X, Li J Q, Zhao Z X and Zheng G Q 2015 *Chin. Phys. Lett.* 32 107401
12. Dong X L, Jin K, Yuan J, Zhou F, Zhang G M and Zhan Z X 2018 *Acta Physica Sinica*, 67 207410
13. Hong X C, Wang A F, Zhang Z, Pan J, He L P, Luo X G, Chen X H and Li S Y 2015 *Chin. Phys. Lett.* 32, 127403
14. Joe Y I, Chen X M, Ghaemi P, Finkelstein K D, de la Pena G A, Gan Y, Lee J C T, Yuan S, Geck J, MacDougall G J, Chiang T C, Cooper S L, Fradkin E and Abbamonte P 2014 *Nat. Phys.* 10 421

15. Yan D, Lin Y S, Wang G H, Zhu Z, Wang S, Shi L, He Y, Li M R, Zheng H, Ma J, Jia J F, Wang Y H and Luo H X 2019 *Supercond. Sci. Technol.* 32 085008
16. Luo H X, Xie W W, Tao J, Inoue H, Gyenis A, Krizan J W, Yazdani A, Zhu Y M and Cava R J 2015 *PNAS* 112 E1174
17. Liu Y, Bao J J, Xu C Q, Jiao W H, Zhang H, Xu C L, Zhu Z, Yang H Y, Zhou Y H, Ren Z, Biswas P K, Ghosh S K, Yang Z, Ke X, Cao G H and Xu X F 2021 *Phy. Rev. B.* 104 104418
18. Xing Y, Yang P, Ge J, Yan J J, Luo J W, Ji H R, Yang Z Y, Li Y J, Wang Z J, Liu Y Z, Yang F, Qiu P, Xi C Y, Tian M L, Liu Y, Lin X and Wang J 2021 *Nano. Lett.* 21 7486
19. Xing Y, Zhao K, Shan P J, Zheng F P, Zhang Y W, Fu H L, Liu Y, Tian M L, Xi C Y, Liu H W, Feng J, Lin X, Ji S H, Chen X, Xue Q K and Wang J 2017 *Nano. Lett.* 17 6802
20. Li X Q, Li Z L, Zhao J J and Wu X S 2020 *Chin. Phys. B* 29 87402
21. Simchi H *Chin. Phys. B* 29 27401
22. Qi Y P, Naumov P G and Ali M N et al. 2016 *Nat. Commun.* 7 11038
23. Chen P, Pa W W, Chan Y H, Takayama A, Xu C Z, Karn A, Hasegawa S, Chou M Y, Mo S K, Fedorov A V and Chiang T C 2017 *Nat. Commun.* 8 516
24. Zhou M H, Li X C and Dong C 2018 *Supercond. Sci. Technol.* 31 065001
25. Luo H X, Xie W W, Tao J, Pletikosic I, Valla T, Sahasrabudhe G S, Osterhoudt G, Sutton E, Burch K S, Seibel E M, Krizan J W, Zhu Y M and Cava R J 2016 *Chem. Mater.* 28 1927
26. Sipos B, Kusmartseva A F, Akrap A, Berger H, Forro L and Tutiš E 2008 *Nat. Mater.* 7 960
27. Ye J T, Zhang Y J, Akashi R, Bahramy M S, Arita R and Iwase Y 2012 *Science* 338, 1193
28. Kusmartseva A F, Sipos B, Berger H, Forró L and Tutiš E 2009 *Phys. Rev. Lett.* 103 236401
29. Fang L, Wang Y, Zou P Y, Tang L, Xu Z, Chen H, Dong C, Shan L and Wen H H 2005 *Phys. Rev. B* 72 014534
30. Hu W Z, Li G, Yan J, Wen H H, Wu G, Chen X H and Wang N L 2007 *Phys. Rev. B* 76 045103
31. Yan D, Wang S, Lin Y S, Wang G H, Zeng Y J, Boubeche M, He Y, Ma J, Wang Y H, Yao D X Luo H X 2020 *J. Phys.: Condens. Matter* 32 025702
32. Kiswandhi A, Brooks J S, Cao H B, Yan J Q, Mandrus D, Jiang Z and Zhou H D 2013 *Phys. Rev. B* 87 121107(R)
33. Zeng J W, Liu E F and Fu Y J et al. 2018 *Nano Lett.* 18 1410
34. Wagner K E, Morosan E, Hor Y S, Tao J, Zhu Y M, Sanders T, McQueen T M, Zandbergen H W, Williams A J, West D V and Cava R J 2008 *Phys. Rev. B* 78 104520
35. Pan X C, Chen X L, Liu H M, Feng Y Q, Wei Z X, Zhou Y H, Chi Z H, Pi L, Yen F, Song F Q, Wan X G, Yang Z R, Wang B G and Zhang Y H 2015 *Nat. Commun.* 6 7805
36. Yu Y J, Yang F Y, Lu X F, Yan Y J, Cho Y H, Ma L G, Niu X H, Kim S, Son Y W,

- Feng D L, Li S Y, Cheong S W, Chen X H and Zhang Y B 2015 *Nat. Nanotech.* 10, 270
37. Luo J W, Li Y A, Zhang J W, Ji H R, Wang H, Shan J Y, Zhang G X, Cai C, Liu J, Wang Y, Zhang Y and Wang J 2020 *Phys. Rev. B* 102 064502
38. Li Y A, Gu Q Q, Chen C, Zhang J, Liu Q, Hu X Y, Liu J, Liu Y, Ling L S, Tian M L, Wang Y, Samarth N, Li S Y, Zhang T, Feng J and Wang J 2018 *P. Natl. Acad. Sci. USA* 115 9503
39. Yan D, Zeng Y J, Wang G H, Liu Y Y, Yin J J, Chang T R, Liu H, Wang M, Ma J, Jia S, Yao D X and Luo H X arXiv:1908.05438
40. Yan D, Zeng L Y, Lin Y S, Yin J J, He Y, Zhang X, Huang M L, Shen B, Wang M, Wang Y H, Yao D X and Luo H X 2019 *Phys. Rev. B* 100 174504
41. Zeng L Y, Yan D, He Y Y, Boubeche M, Huang Y H, Wang X P and Luo H X 2021 *J. Alloy. Compd.* 885, 160981
42. Boubeche M, Yu J, Li C S, Wang H C, Zeng L Y, He Y Y, Wang X P, Su W Z, Wang M, Yao D X and Luo H X 2021 *Chin. Phys. Lett.* 38 037401
43. Boubeche M, Wang N N, Sun J P, Yang P T, Zeng L Y, Li Q Z, He Y Y, Luo S J, Cheng J G, Peng Y Y and Luo H X 2021 *Supercond. Sci. Tech.* 34 115003
44. Antal V, Kanuchova M, Šefčíková, M, Kovac J, Diko P, Eisterer M, Hörhager N, Zehetmayer M, Weber H W and Chaud X 2009 *Supercond. Sci. Technol.* 22 105001
45. Scavini B, Malavasi L and Mollica L 2004 *Solid. State. Sci.* 6 1187
46. Ansari I 2017 *J. Mod. Mater.* 3 33
47. Ginzburg V L and Landau L D 1950 *Zh. Eksp. Teor. Fiz.* 20 1064
48. McMillan W L 1968 *Phys. Rev. B* 167, 331
49. Bardeen J, Cooper L N and Schrieffer J R 1957 *Phys. Rev.* 108 1175